



OPEN

Multi-band terahertz anisotropic metamaterial absorber composed of graphene-based split square ring resonator array featuring two gaps and a connecting bar

Somayyeh Asgari[✉] & Tapio Fabritius

A multi-band anisotropic metamaterial absorber operating in the terahertz (THz) range is constructed using a graphene-based split square ring resonator array featuring two gaps and a connecting bar. The design is meticulously simulated through the finite element method (FEM) using CST Software. Subsequently, an equivalent circuit model (ECM) is introduced, leveraging impedance and transmission lines, and implemented with a rapid MATLAB code to evaluate the absorber's behavior in the THz spectrum. The proposed absorber, dynamically adjustable through a one-layered resonator array, exhibits a strong linear dichroism response of 99% within a frequency range of 0.3–4 THz. The metamaterial has an absorption rate of 81% for one absorption band in transverse magnetic mode and its three absorption bands in transverse electric mode have an average of 99.3% in each absorption band with absorption over 99%. This absorber holds potential applications in polarization-sensitive devices and THz systems. The ECM model was established to provide an efficient analytical tool for assessing the absorber's performance, and the FEM simulation results align well with those derived from the ECM.

Anisotropic metamaterials exhibit non-equal responses to the incident waves along some different directions. Metamaterials fall into the category of anisotropic metamaterials if they possess at least one of the following features: anisotropic geometries, anisotropic material within the metamaterial structure, or applying an external magnetic field to the metamaterial. Metamaterials featuring anisotropic geometries do not coincide with their mirror image at some rotational angles¹.

Graphene, which is a two-dimensional layer derived from graphite, possesses exceptional qualities that render it a favorable option for optical devices and systems. Recently, there have been proposals, analyses, and investigations into anisotropic metamaterials based on graphene. These metamaterials demonstrate tunable anisotropic responses like linear dichroism (LD)^{2–5}. Tunable graphene-based terahertz (THz) anisotropic metamaterials can find potential applications in polarization-sensitive devices and systems.

Through the adjustment of the graphene-based metamaterial absorber's spectral response by the alternation of the applied bias voltage dynamically, graphene-based multi-band absorbers can be employed in a variety of applications. They can be used to reduce electromagnetic interference for next-generation (6G) wireless communication multi-channel systems by absorbing undesired electromagnetic radiation⁶. Moreover, they have the potential to play a crucial role in advancing telecommunication multi-channel systems in the future. In addition to multi-channel telecommunication systems⁷ these multi-band metamaterial absorbers can be used in highly sensitive and selective sensing and imaging, spectroscopy applications^{8–13}, filtering¹⁰, switching¹², modulation¹³, energy absorbing and energy converting¹⁴, power detecting¹⁵, power receiving¹⁶, and more. However, most of the earlier reported structures have limited number of absorption peaks thus hindering their usability in some applications.

Creating multi-channel systems involves constructing components with multiple absorption bands. Metamaterials commonly achieve this by integrating either multiple layers of resonators or super unit cells to encompass a multi-band spectrum of absorption bands^{17–19}. Graphene-based anisotropic metamaterials reported in^{2,5} are

Optoelectronics and Measurement Techniques Research Unit, Faculty of Information Technology and Electrical Engineering, University of Oulu, Oulu, Finland. ✉email: somayyeh.asgari@oulu.fi

dual-band THz absorbers. The absorber in² has two layers of resonators each layer containing one resonator and the absorber in⁵ has two resonators in one layer of resonator. To increase the number of absorption peaks without compromising with simplicity of the structure, the aim of this work was to design a multi-band THz graphene-based anisotropic metamaterial absorber containing simple geometry with few resonator layers and few resonators per unit cell.

There is one paper reporting four THz graphene-based multi-band metamaterial absorbers composed of square split ring resonator arrays with different number of gaps²⁰. The absorbers were designed in 0.1–5.5 THz with limited maximum absorption and limited maximum LD response. In this paper, we have designed and developed a multi-band THz graphene-based anisotropic metamaterial absorber which is composed of a square split ring resonator array featuring two gaps and a connecting bar, with increased absorption, LD, and number of absorption bands. In addition, the ECM in this work differs from that reported in²⁰.

Materials and methods

Figure 1 illustrates the metamaterial absorber configuration from various perspectives, including periodic, unit cell, front, and side views. The layers making the metamaterial from the top to the bottom are respectively ion gel, graphene, Rogers RT5880LZ, and gold. Atop the metamaterial structure, there is a layer of ion gel with a permittivity value of $\epsilon_{ig} = 2.0164$ and a thickness of 150 nm. The primary function of this ion gel layer is to apply bias to the underlying graphene resonator layer²¹.

The metamaterial is composed of a gold layer with high conductivity ($\sigma = 4.56 \times 10^7$ S/m)²². The maximum penetration depth ($\delta_{max} = \sqrt{\frac{1}{\sigma \pi f_{min} \mu_r \mu_0}}$) for the gold layer happens in 0.3 THz (minimum frequency f_{min} of the frequency range) where the relative permeability μ_r is 1 and vacuum permeability μ_0 is $4\pi \times 10^{-7}$. So, the maximum penetration depth is 0.1361 μm . The gold layer with a thickness of 0.5 μm which is much larger than the penetration depth ($\sim 3.7 \times$ maximum penetration depth) of the THz waves is selected to ensure that the incident electromagnetic wave cannot transmit to the other side of the absorber and the transmission is zero because the electromagnetic waves can penetrate inside the gold layer up to its penetration depth²³. The gold layer acts as a perfect reflector for the considered THz design range. Moreover, it doesn't produce any loss since it has a big conductivity and energy cannot go through it²⁴. Positioned on this gold layer is a dielectric layer, on which graphene patterns are arranged. In this configuration, graphene is depicted as an extremely thin layer ($\Delta = 0.335$ nm) embedded within Rogers RT5880LZ. Rogers RT5880LZ has a permittivity value of $\epsilon_d = 2$. The design also incorporates a graphene-based split square ring resonator array, featuring two gaps and a connecting bar, situated on the dielectric layer.

Fabrication of the metamaterial is not in the scope of this work, but we briefly summarize the fabrication process here for future readers of the work who may want to fabricate this metamaterial: Begin by applying a 13 μm thick dielectric with gold coating on one side through chemical vapor deposition (CVD)²⁵. Subsequently, use a standard lithography process to create the graphene patterns on the dielectric²⁶. Transfer the ion gel dielectric onto the graphene resonator array using thermal evaporation²⁷.

Dimensional and material parameters of the metamaterial of Fig. 1 are optimized. $d_{ion-gel}$ is the thickness of the ion gel layer = 150 nm, $d_{substrate}$ is the thickness of the dielectric substrate = 13 μm , d_{gold} is the thickness of the gold layer = 0.5 μm , P_x is the unit cell dimension in x direction = 16 μm , P_y is the unit cell dimension in y

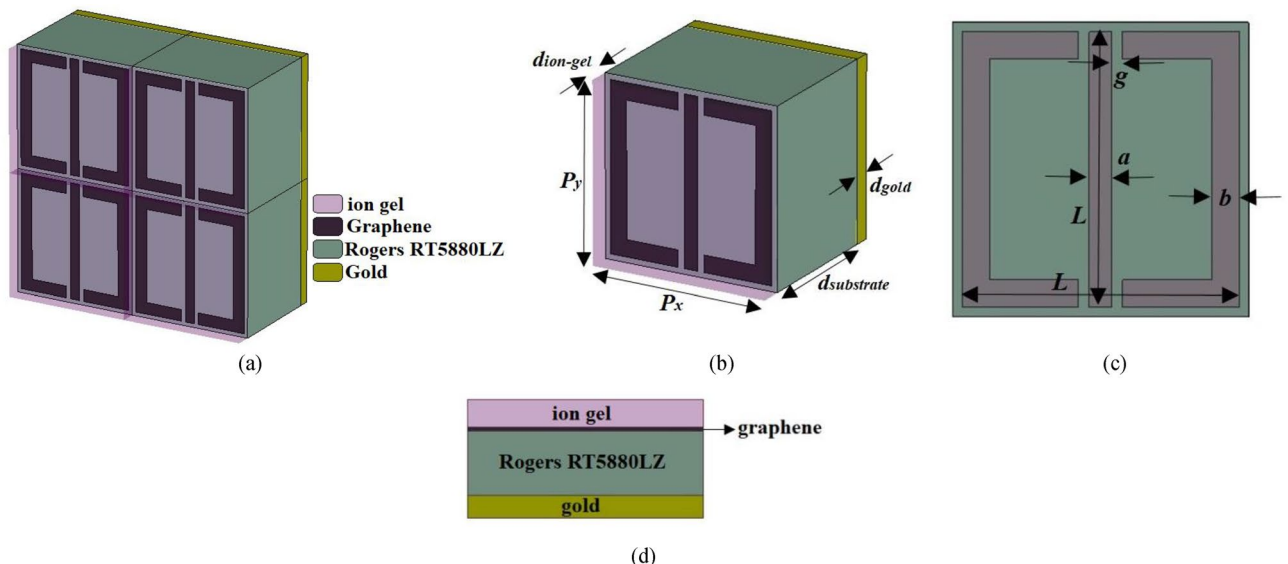


Figure 1. (a) Periodic, (b) unit cell, (c) front, and (d) side views of the proposed multi-band terahertz anisotropic metamaterial absorber which is comprised of a graphene-based split square ring resonator array with two gaps and a bar between the gaps. The layers making the metamaterial from the top to the bottom are respectively ion gel, graphene, Rogers RT5880LZ, and gold. We have used a layer of ion gel to bias the resonator array and a gold layer beneath the metamaterial to avoid the transmission of electromagnetic waves.

direction = $16 \mu\text{m}$, a is the width of connecting bar = $1.2 \mu\text{m}$, L is the length of connecting bar and outer length of split square ring = $15 \mu\text{m}$, g is the gap distance = $0.6 \mu\text{m}$, b is the width of split square ring = $1.5 \mu\text{m}$, E_f is the Fermi energy level of graphene = 1 eV , and τ is the relaxation time of graphene = 2 ps .

Numerical simulations were conducted using the finite element method (FEM) with the frequency domain solver in CST Microwave Studio^{5,20,28–30}. Periodic (unit cell) boundary conditions were applied in the x and y directions, while an absorbing (open (add space)) boundary condition was implemented in the z direction. The metamaterial was meshed using a tetrahedral mesh^{5,20,29,30}. Optimization of the metamaterial was performed using the genetic algorithm (the parameter values were randomly changed to find the optimal values) within the CST software^{5,20,30–32}. The unit cell dimensions were set as $P_x = P_y = 16 \mu\text{m}$, a size smaller than $\lambda_{\text{min}} = 75 \mu\text{m}$, which corresponds to $f_{\text{max}} = 4 \text{ THz}$, the upper limit of the simulated frequency range. This sizing decision was made to prevent the propagation of higher-order Floquet modes^{5,20,30,33,34}.

The total thickness of the metamaterial, including the ion gel, graphene, Rogers RT5880LZ, and gold layers, was $13.65 \mu\text{m}$, approximately $0.182 \times \lambda_{\text{min}}$ which shows that the metamaterial is relatively thin in the simulated frequency range^{5,30}. The relative permittivity and the surface conductivity of graphene are modeled as reported in^{5,20}.

As is clear in Fig. 1, the graphene-based resonator array is composed of the graphene-based split ring resonator array and the graphene-based middle connecting bar array. As shown in Fig. 2a,b, the impedance of the split ring resonator array is considered as Z_1 , and the impedance of the middle connecting bar array is assumed as Z_2 . The split ring resonator array consists of horizontal and vertical arms as shown in Fig. 2a. The ECM of the graphene-based resonator array in TE and TM modes are respectively given in Fig. 2c,d.

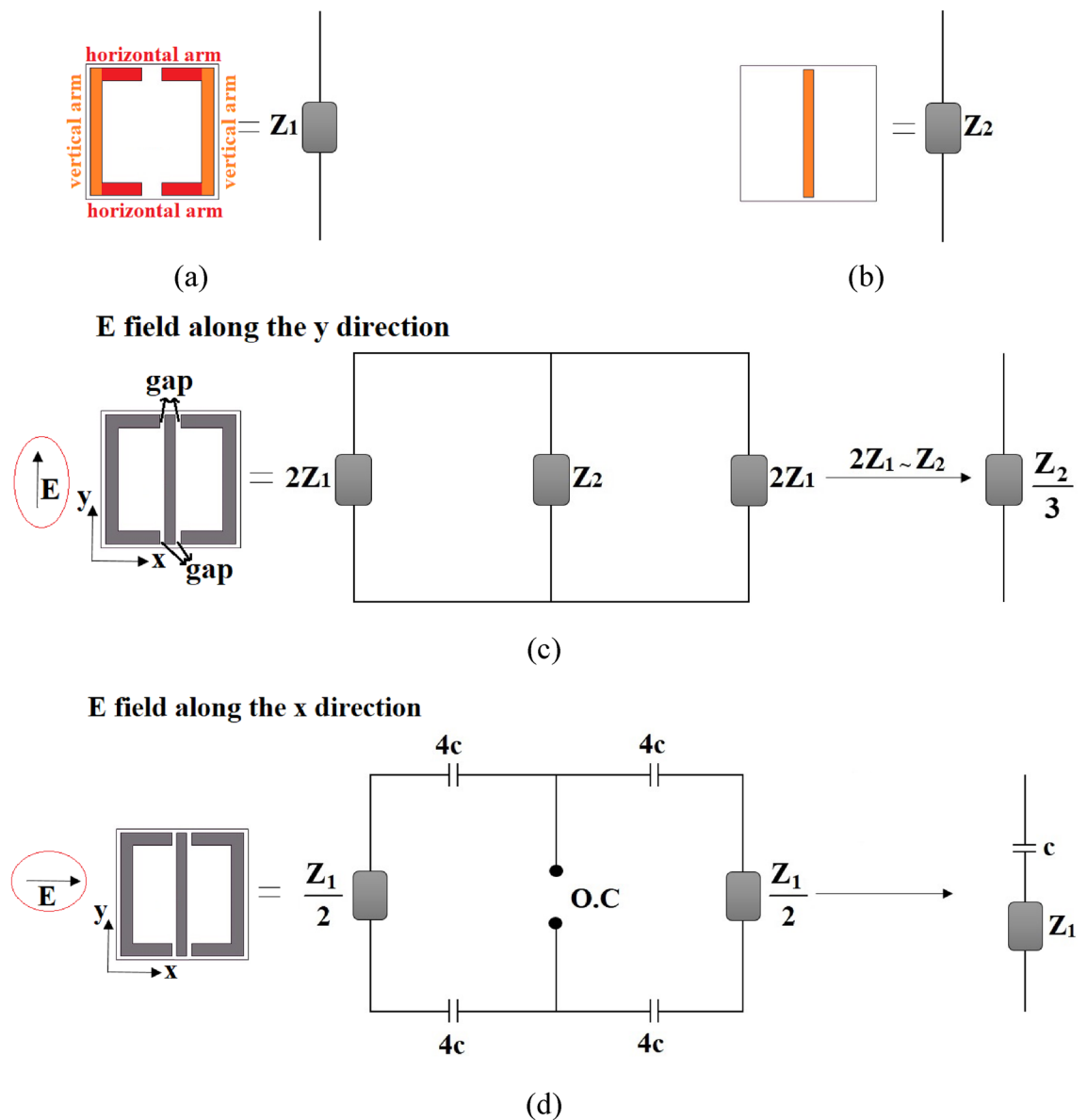


Figure 2. Equivalent circuit model (ECM) of the (a) graphene-based split ring resonator array composing of horizontal and vertical arms, (b) graphene-based middle connecting bar array, and graphene-based resonator array layer in (c) TE (E field along the y direction) and (d) TM (E field along the x direction) modes.

The graphene resonator layer has a non-symmetric geometry so the ECMs in TE and TM modes differ. For TE mode (Fig. 2c), the incident E field is along the y direction. There are four gaps between the middle connecting bar and the split ring resonator (shown in Fig. 2c). The E field is parallel to the gaps, so the gaps are not modeled. E field is along the middle connecting bar, so it's modeled by Z_2 . The split ring resonator is modeled by Z_1 and each half of the split ring resonator is modeled by $2Z_1$. As depicted in Fig. 2c, the anisotropic metamaterial contains three parallel impedances in TE mode. So, the impedance in TE mode Z_{TE} is calculated by:

$$Z_{TE} = \frac{Z_1 Z_2}{Z_1 + Z_2} \quad (1)$$

Since the E field is along the y direction, the produced impedance by the horizontal arms (shown in Fig. 2a) of the split ring resonator is very small and neglected (the width of the arms is much smaller than their length). Each vertical arm (shown in Fig. 2a) of the split ring resonator produces $2Z_1$ and they have equal length and width with the middle connecting bar, so they have equal impedances:

$$2Z_1 \sim Z_2 \quad (2)$$

So:

$$Z_{TE} = \frac{Z_2}{3} \quad (3)$$

For TM mode (Fig. 2d), the incident E field is along the x direction. The E field is normal to the gaps, so the gaps are modeled by capacitors and each capacitor is assumed to have a capacitance of $4c$. E field is not along the middle connecting bar, so it's modeled as an open circuit (O.C). The split ring resonator is modeled by Z_1 and each half of the split ring resonator is modeled by $Z_1/2$. The ECM in TM mode simplifies to a series of Z_1 and c .

The effective conductivity of the graphene resonator layer by Fresnel equation in TE mode can be obtained by³⁵:

$$\sigma_{TE} = \frac{\cos(\theta_{in}) - \sqrt{\epsilon_d} \cos(\theta_{out}) - r^{TE} (\cos(\theta_{in}) + \sqrt{\epsilon_d} \cos(\theta_{out}))}{Z_0 (1 + r^{TE})} \quad (4)$$

in which θ_{in} , ϵ_d , θ_{out} , r^{TE} , and Z_0 are respectively the angle of the incident illuminated wave, the relative permittivity of the dielectric substrate, angle of the transmitted wave, the reflection coefficient of the graphene resonator layer in TE mode, and the vacuum impedance. The relation between θ_{in} and θ_{out} is:

$$\sin(\theta_{out}) = \sqrt{\frac{1}{\epsilon_d}} \sin(\theta_{in}) \quad (5)$$

Impedance is the inverse of conductivity (admittance). So²⁰:

$$Z_{TE} = \frac{1}{\sigma_{TE}} \quad (6)$$

By substituting Eq. (6) in Eq. (3), we have:

$$Z_2 = \frac{3}{\sigma_{TE}} \quad (7)$$

which is equal to:

$$Z_2 = \frac{3Z_0(1 + r^{TE})}{\cos(\theta_{in}) - \sqrt{\epsilon_d} \cos(\theta_{out}) - r^{TE} (\cos(\theta_{in}) + \sqrt{\epsilon_d} \cos(\theta_{out}))} \quad (8)$$

As shown in Fig. 2b, the graphene resonator array in TM mode is modeled by a series circuit containing Z_1 and c . So:

$$Z_{TM} = Z_c + Z_1 \quad (9)$$

where Z_c is the impedance of the capacitor. Also²⁰:

$$Z_{TM} = \frac{1}{\sigma_{TM}} \quad (10)$$

The effective conductivity of the graphene resonator layer by Fresnel equation in TM mode can be obtained by³⁵:

$$\sigma_{TM} = \frac{\sec(\theta_{in}) - \sqrt{\epsilon_d} \sec(\theta_{out}) - r^{TM} (\sec(\theta_{in}) + \sqrt{\epsilon_d} \sec(\theta_{out}))}{Z_0 (1 + r^{TM})} \quad (11)$$

where r^{TM} is the reflection coefficient of the graphene resonator layer in TM mode. The impedance of the gap capacitance can be obtained by²⁰:

$$Z_c = \frac{1}{j\omega c} \tag{12}$$

where ω is the angular frequency. The gap capacitance is calculated by:

$$c = \epsilon_{\text{eff}} \frac{b}{g} \tag{13}$$

where ϵ_{eff} is the effective permittivity calculated by²⁰:

$$\epsilon_{\text{eff}} = \epsilon_0 \frac{1 + \epsilon_d}{2} \tag{14}$$

in which ϵ_0 is the permittivity of vacuum. Substituting Eqs. (13) and (14) in Eq. (12), we will have:

$$Z_c = \frac{2g}{j\omega b\epsilon_0(1 + \epsilon_d)} \tag{15}$$

Then, Z_1 can be calculated from:

$$Z_1 = \frac{Z_0(1 + r^{TM})j\omega\epsilon_0(1 + \epsilon_d) - 2w[\sec(\theta_{\text{in}}) - \sqrt{\epsilon_d} \sec(\theta_{\text{out}}) - r^{TM}(\sec(\theta_{\text{in}}) + \sqrt{\epsilon_d} \sec(\theta_{\text{out}}))]}{j\omega\epsilon_0(1 + \epsilon_d)[\sec(\theta_{\text{in}}) - \sqrt{\epsilon_d} \sec(\theta_{\text{out}}) - r^{TM}(\sec(\theta_{\text{in}}) + \sqrt{\epsilon_d} \sec(\theta_{\text{out}}))]} \tag{16}$$

The entire metamaterial is represented by transmission lines, as depicted in Fig. 3. The input impedances for each segment of the metamaterial absorber are illustrated in the same figure. Given that the thickness of the graphene layer is significantly smaller than the minimum wavelength within the simulated wavelength range, the graphene resonator layer is simplified and modeled as a point load^{36,37}.

The input impedances of the different segments of Fig. 3 are calculated by^{20,36}:

$$Z_1^{TE/TM} = Z_d^{TE/TM} \frac{Z_{Au} + jZ_d^{TE/TM} \tan(\beta_d d)}{Z_d^{TE/TM} + jZ_{Au} \tan(\beta_d d)} \tag{17}$$

in which $Z_d^{TE/TM}$ and β_d are respectively the TE/TM impedances of the dielectric substrate and the propagation constant of the THz electromagnetic wave in the dielectric substrate.

Since the conductivity of gold is high and its thickness is much larger than the maximum penetration depth of electromagnetic waves in the designed frequency range, the waves cannot transmit through the gold layer to the other side of the metamaterial. So, it acts as a perfect reflector and its impedance can be considered as zero, $Z_{Au} = 0$. Then, Eq. (17) is simplified to^{20,36}:

$$Z_1^{TE/TM} = jZ_d^{TE/TM} \tan(\beta_d d) \tag{18}$$

$$Z_2^{TE/TM} = Z_g^{TE/TM} \parallel Z_1^{TE/TM} \tag{19}$$

where $Z_g^{TE/TM}$ is the TE/TM impedances of the graphene resonator layer. The input impedance of the metamaterial can be obtained by^{20,36}:

$$Z_{\text{in}}^{TE/TM} = Z_{\text{ig}}^{TE/TM} \frac{Z_2^{TE/TM} + jZ_{\text{ig}}^{TE/TM} \tan(\beta_{\text{ig}} d_{\text{ig}})}{Z_{\text{ig}}^{TE/TM} + jZ_2^{TE/TM} \tan(\beta_{\text{ig}} d_{\text{ig}})} \tag{20}$$

in which $Z_{\text{ig}}^{TE/TM}$ and β_{ig} are respectively the TE/TM impedances of the ion gel layer and the propagation constant of the THz electromagnetic wave in the ion gel²⁰.

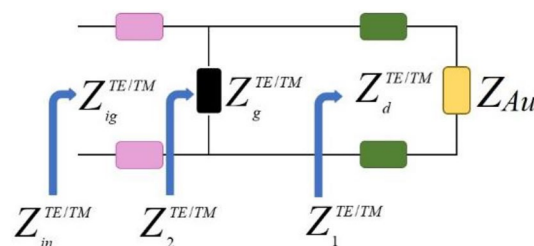


Figure 3. ECM of the whole metamaterial absorber.

$$Z_{ig/d}^{TE} = \frac{Z_0}{\sqrt{\epsilon_{ig/d}}} \cos(\theta_{in/d}) \tag{21}$$

$$Z_{ig/d}^{TM} = \frac{Z_0}{\sqrt{\epsilon_{ig/d}}} \sec(\theta_{in/d}) \tag{22}$$

in which θ_d is the electrical length of the substrate²⁰.

$$\theta_d = \frac{d_{\text{substrate}} \omega \sqrt{\epsilon_d}}{c} \tag{23}$$

$$\beta_{ig/d} = \frac{\omega \sqrt{\epsilon_{ig/d}}}{c} \tag{24}$$

The TE/TM scattering parameters (return losses) of the metamaterial $S_{11}^{TE/TM}$ can be obtained by²⁰:

$$S_{11}^{TE} = \frac{Z_{in}^{TE} - Z_0 \cos(\theta_{in})}{Z_{in}^{TE} + Z_0 \cos(\theta_{in})} \tag{25}$$

$$S_{11}^{TM} = \frac{Z_{in}^{TM} - Z_0 \sec(\theta_{in})}{Z_{in}^{TM} + Z_0 \sec(\theta_{in})} \tag{26}$$

in which $Z_{in}^{TE/TM}$ is obtained from Eq. (20). The TE/TM reflections of the metamaterial $R^{TE/TM}$ are obtained by^{20,38}:

$$R^{TE/TM} = \left| S_{11}^{TE/TM} \right|^2 \tag{27}$$

Since the metamaterial is backed by a gold layer, there is zero transmission ($T^{TE/TM} = 0$) for the metamaterial. So, the insertion losses ($T^{TE/TM}$ or $S_{21}^{TE/TM}$) for TE/TM modes are zero³⁸. The TE/TM absorptions of the metamaterial $A^{TE/TM}$ are obtained by^{20,38}:

$$A^{TE/TM} = 1 - R^{TE/TM} \tag{28}$$

The linear dichroism (LD) is the difference in absorbance for TE and TM polarized waves^{5,20,38}:

$$LD = A^{TM} - A^{TE} \tag{29}$$

Results and discussion

Absorption spectra of the anisotropic metamaterial absorber of Fig. 1 for both TE and TM mode are obtained by CST and the results are shown in Fig. 4. The metamaterial has different responses for TE and TM waves, and it works in 0.3–4 THz. There are three resonances in TE mode with average absorption of 99.3% and one resonance in TM mode with absorption rate of 81%.

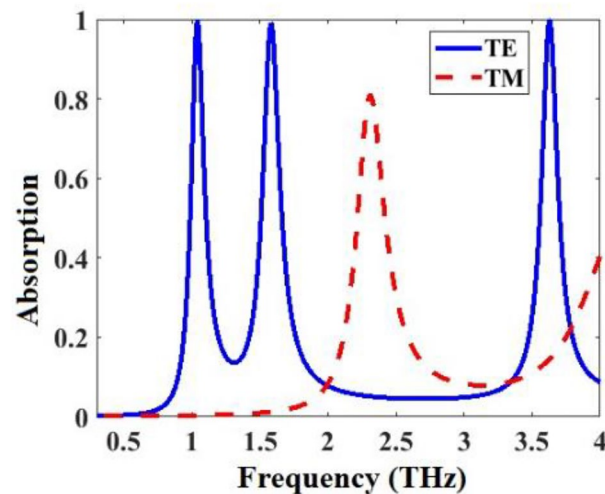


Figure 4. TE and TM absorption spectra of the anisotropic metamaterial absorber of Fig. 1.

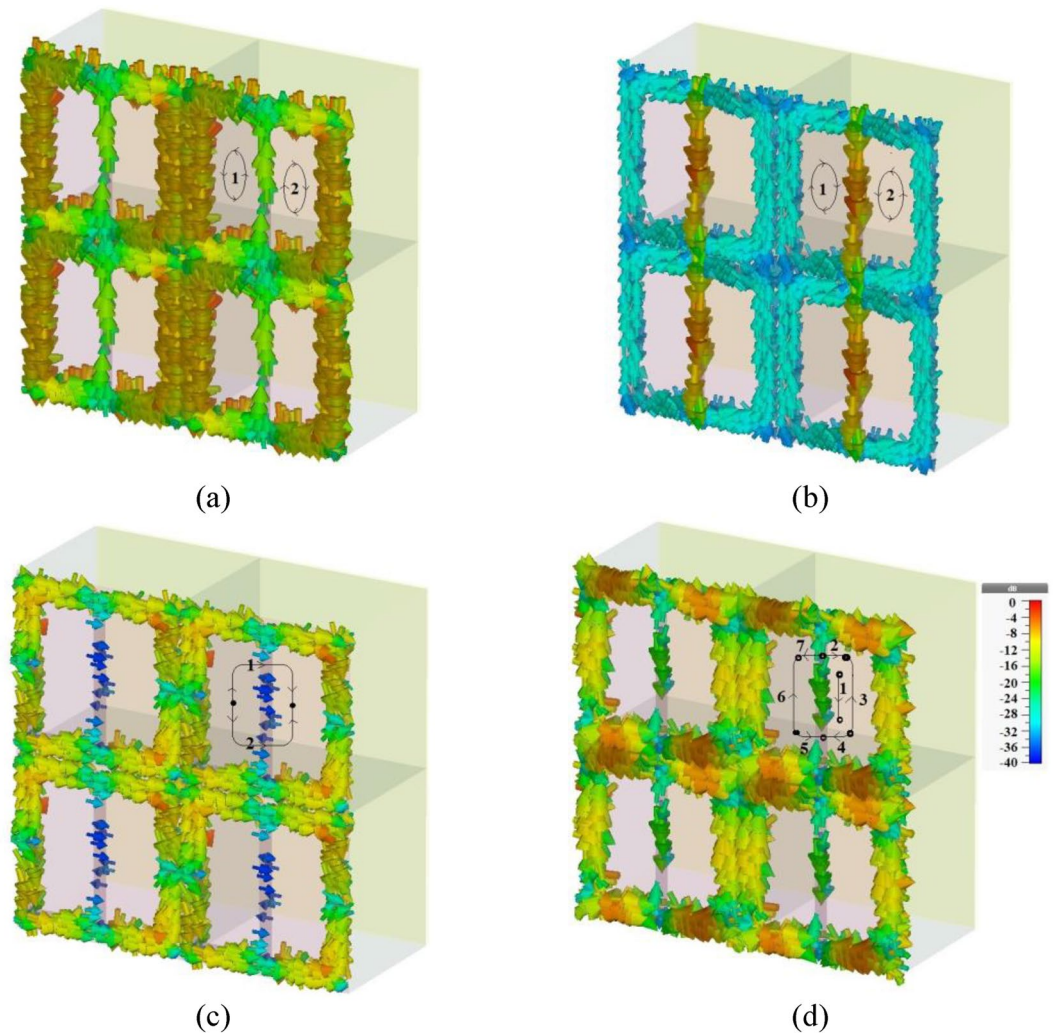


Figure 5. Surface current distributions of the metamaterial absorber of Fig. 1 in (a) 1.04, (b) 1.58, (c) 2.31, and (d) 3.63 THz.

Surface current distributions in the resonance frequencies of the anisotropic metamaterial absorber of Fig. 1 are displayed in Fig. 5. In 1.04 THz, the surface currents make two loops (two magnetic dipoles), one of them anticlockwise and the other one clockwise. In 1.58 THz, the surface currents also make two loops (two magnetic dipoles), one of them clockwise and the other one anticlockwise. In 2.31 THz, the surface currents make two electric dipoles with the directions shown in Fig. 5c. In 3.63 THz, the surface currents make seven electric dipoles with the directions shown in Fig. 5d.

To start the ECM analysis, the graphene resonator layer is placed on the dielectric with thickness of 300 μm which is considered as a half-space to minimize the influence of the substrate on the impedances of the graphene resonator layer. The configuration is simulated in CST and the reflection spectra are obtained. The obtained TE and TM reflection spectra (r^{TE} in Eq. (4) and r^m in Eq. (11)) are given in Fig. 6a,b. Then, Eqs. (4) and (11) are calculated to obtain the equivalent conductivities of the graphene resonator layer in TE and TM modes, and the results are given in Fig. 6c–f. The real parts are positive (Fig. 6c,d) representing the resistive nature and the imaginary parts contain both positive and negative sections (Fig. 6e,f) indicating the inductive and capacitive natures of the graphene resonator array.

The resonator array of the metamaterial of Fig. 1 consists of a split ring resonator array Z_1 and the middle connecting bar array Z_2 . We have calculated and plotted the real and imaginary parts of the impedances of these arrays separately and the results are given in Fig. 7. Z_1 and Z_2 are shown in the inset figures in Fig. 7. The real parts are positive producing great loss, and the imaginary parts contain both positive and negative sections indicating the inductive and capacitive natures of the split ring resonator array and the middle connecting bar array.

TE and TM absorption spectra of the metamaterial absorber of Fig. 1 for three different values of incident angle θ_{in} are respectively given in Fig. 8a,b. By change of θ_{in} , As shown, by change of θ_{in} , the absorption spectra for both modes alter slightly so the metamaterial is incident angle independent.

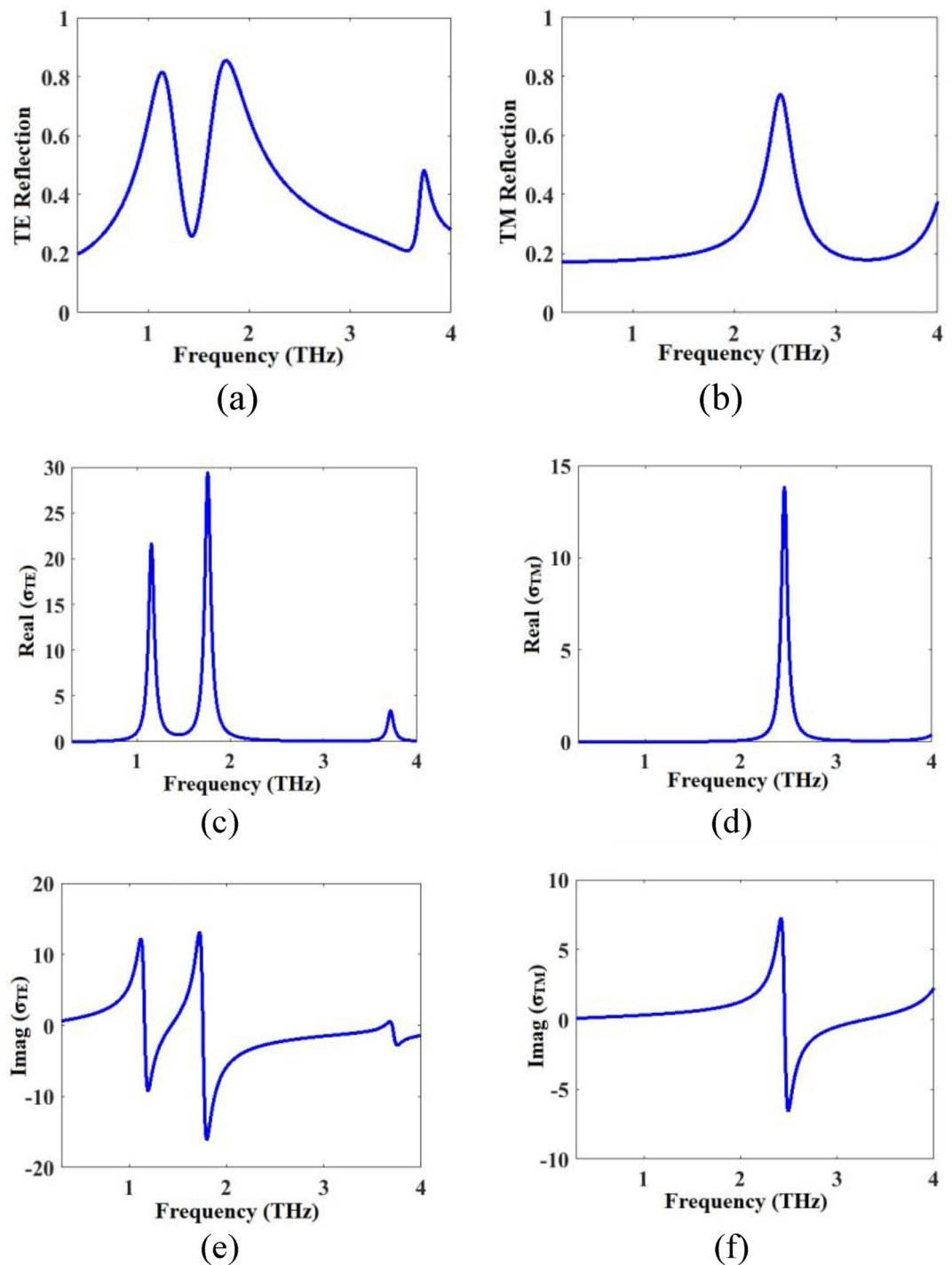


Figure 6. (a) TE and (b) TM reflection spectra of the graphene-based resonator array layer when its located on the half-space substrate without considering the ion gel and gold layers. (c) and (d) real, (e) and (f) imaginary parts of the equivalent conductivity of the graphene resonator array layer in TE and TM modes (Eqs. (10) and (11)).

TE and TM absorption spectra for the metamaterial of Fig. 1 obtained by CST and ECM for three different values of θ_{in} are given in Fig. 9. Obtained spectra with both methods are in good agreement and the ECM works for any oblique incident angle of the illuminated wave θ_{in} .

The real and imaginary parts of the normalized input impedances in TE and TM modes (Z_{in}^{TE}/Z_0 and Z_{in}^{TM}/Z_0) of the proposed anisotropic metamaterial absorber of Fig. 1 with the properties presented in Fig. 9a,b are shown in Fig. 10a,b, respectively. Z_0 is the vacuum impedance equal to 377Ω .

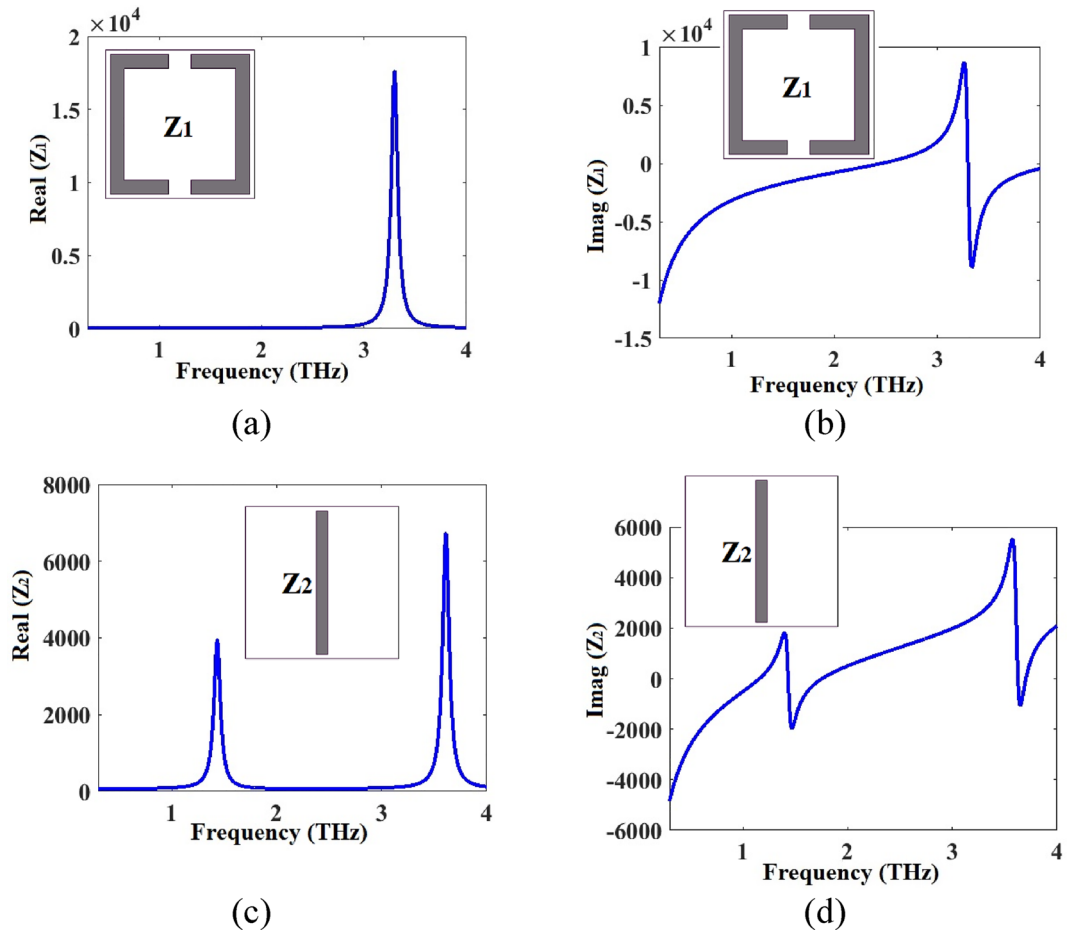


Figure 7. (a) Real and (b) imaginary parts of Z_1 (impedance of the split ring resonator array of the metamaterial of Fig. 1 as shown in the inset figure). (c) Real and (d) imaginary parts of Z_2 (impedance of the middle connecting bar array of the metamaterial of Fig. 1 as shown in the inset figure).

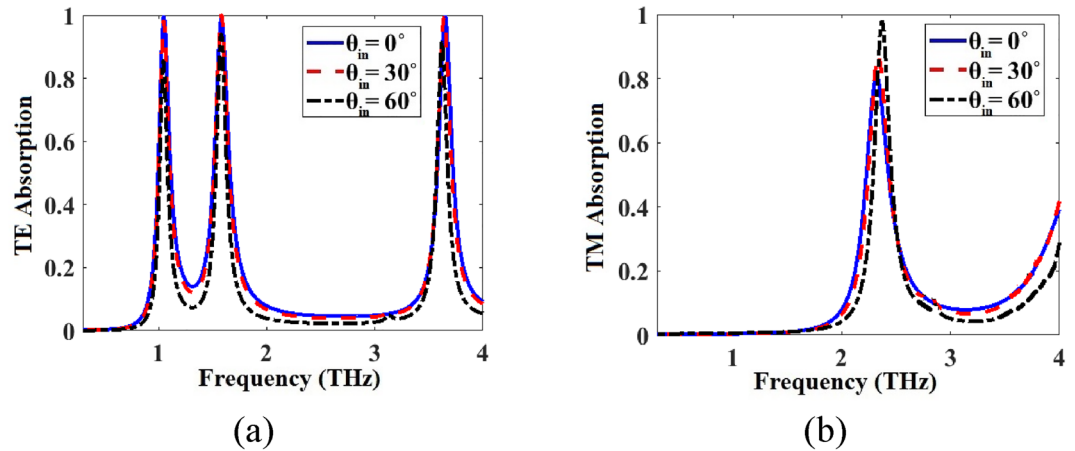


Figure 8. (a) TE and (b) TM absorption spectra of the metamaterial absorber of Fig. 1 for three different values of incident angle θ_{in} .

As shown in the curve obtained by ECM in Fig. 9a, absorption peaks in the first and second peaks reach 1 while the absorption in the third peak reaches 0.8. As shown in Fig. 10a, the imaginary part of the normalized input impedance is zero at the first and second absorption peaks and 0.27 at the third absorption peak. Also, the real part approaches 1 in the first and second peaks while 0.82 in the third peak. As shown in the curve obtained by ECM in Fig. 9b, absorption peak reach 1. As shown in Fig. 10b, the imaginary part of the normalized input

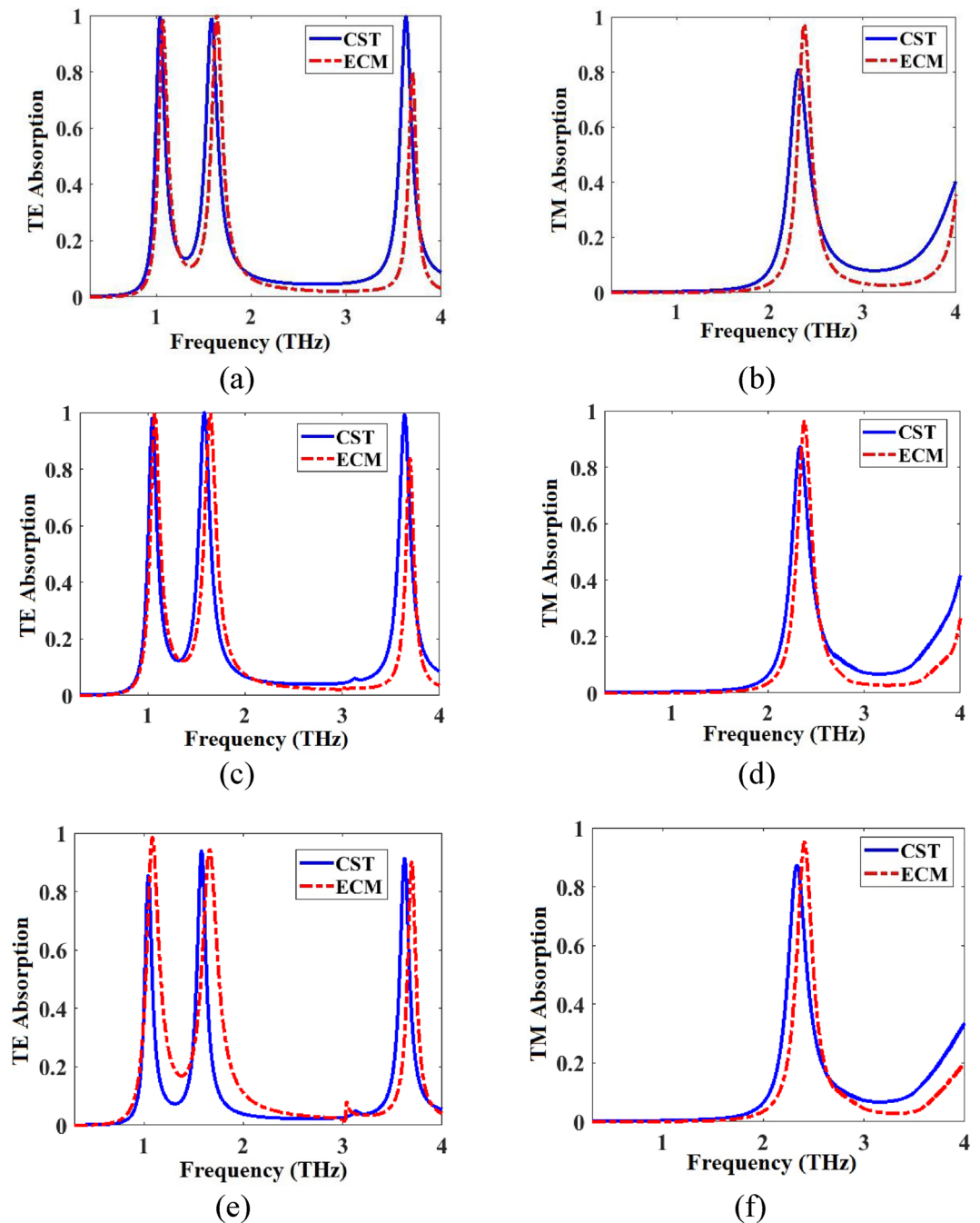


Figure 9. Absorption spectra of the metamaterial absorber of Fig. 1 obtained by CST and ECM in (a) TE mode for $\theta_{in}=0$, (b) TM mode for $\theta_{in}=0$, (c) TE mode for $\theta_{in}=30$, (d) TM mode for $\theta_{in}=30$, (e) TE mode for $\theta_{in}=60$, and (f) TM mode for $\theta_{in}=60$.

impedance is zero at the absorption peak. Also, the real part approaches 1 in the absorption peak. These characteristics show the impedance matching condition to achieve the perfect absorption at the resonance peaks (Fig. 10).

The linear dichroism (LD: the difference in absorbance for TE and TM polarized waves) vs frequency for the metamaterial of Fig. 1 obtained by Eq. (29) for three different values of graphene Fermi energy E_f are shown in Fig. 11. The maximum LD reaches 99% for this metamaterial. By increasing of E_f , the resonance frequencies of the LD spectra increase, showing a blueshift. This is because the real part of the β decreases as the E_f increases (Eq. (4) in²⁰). So, the resonances increase with the increase of E_f .

The results of this work are compared with some previously published works in Table 1. The performance of the metamaterial in this work is improved compared to the metamaterial containing of two gaps (without the connecting bar) in²⁰.

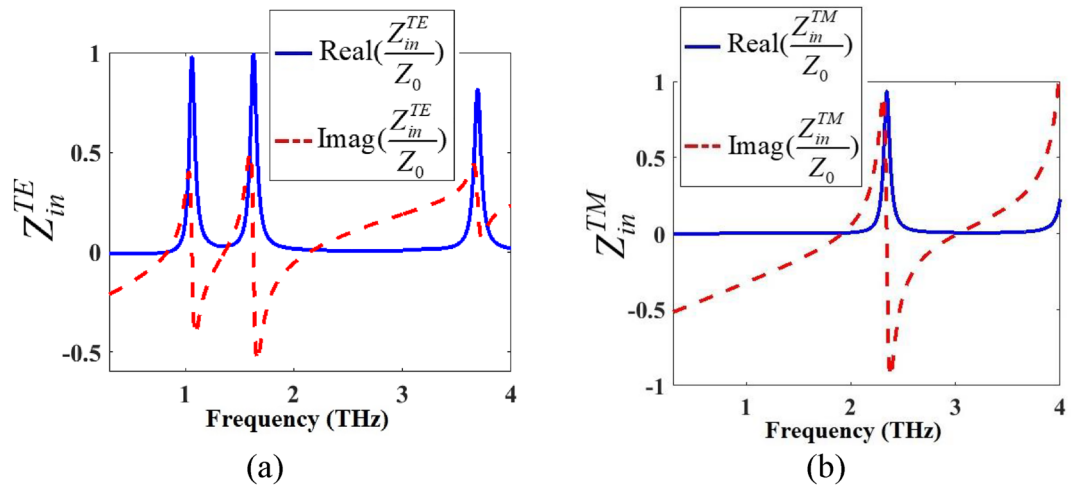


Figure 10. Normalized input impedance of the anisotropic metamaterial absorber of Fig. 1 in (a) TE and (b) TM modes with properties respectively presented in Fig. 9a,b.

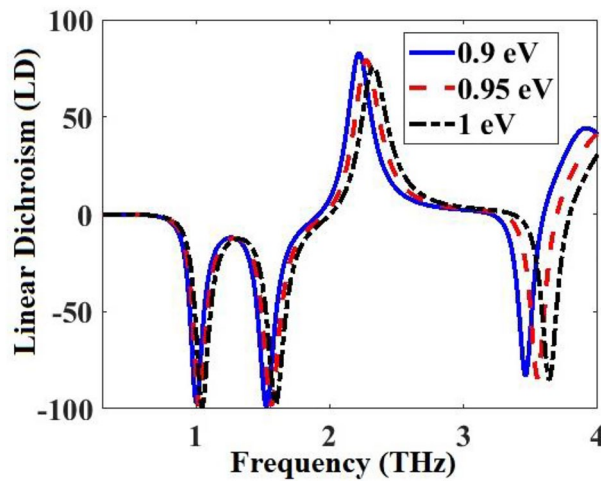


Figure 11. Linear dichroism (LD: the difference in absorbance for TE and TM polarized waves) of the metamaterial absorber of Fig. 1 obtained by Eq. (29) for three different values of graphene Fermi energy E_f .

	Frequency range (THz)	Max. absorption (%)	Max. linear dichroism (LD)	Max. number of absorption bands
⁵	0.1–5.5	100	100	Two
²⁰ one gap structure	1–5.5	98.8	94	Three
²⁰ two gaps structure	1–5.5	99	93	Two
²⁰ three gaps structure	1–5.5	98.6	87	Three
²⁰ four gaps structure	1–5.5	88.4	73	Three
³⁹	0.5–1.5	100	90	One
This work	0.3–4	100	99	Three

Table 1. Comparison of this work with some previously published works.

Conclusion

In this study, we propose an Equivalent Circuit Modeling (ECM) approach utilizing impedance and transmission lines, implemented through a straightforward MATLAB code. The focus is on a terahertz (THz) graphene absorber with a graphene-based split square ring resonator array, featuring two gaps and a connecting bar. The design is subjected to numerical simulation using CST Microwave Studio Software, employing the finite element method (FEM). The results from both FEM and ECM exhibit good agreement. The absorber design is

dynamically tunable, comprising a one-layer resonator array with two resonators per unit cell. The metamaterial absorber demonstrates a pronounced linear dichroism (LD) response, achieving 99% efficiency. The metamaterial has an absorption rate of 81% for one absorption band in transverse magnetic (TM) mode. Its three absorption bands in transverse electric (TE) mode have an average of 99.3% in each absorption band with absorption over 99%. This delineates a single absorption band for TM mode and three for TE mode. The proposed graphene absorber holds promise as a component in polarization-sensitive systems for controllable absorption and sensing applications.

Data availability

The datasets generated and/or analysed during the current study are available from the corresponding author on reasonable request.

Received: 10 January 2024; Accepted: 26 March 2024

Published online: 29 March 2024

References

- Albooyeh, M. *et al.* Classification of bianisotropic metasurfaces from reflectance and transmittance measurements. *ACS Photonics* **10**, 71–83 (2023).
- Li, J. *et al.* Polarization-dependent and tunable absorption of terahertz waves based on anisotropic metasurfaces. *Opt. Express* **29**, 3284–3295 (2021).
- Zhang, C. *et al.* Graphene-based anisotropic polarization meta-filter. *Mater. Des.* **206**, 109768 (2021).
- Wu, F., Liu, D., Wu, X., Li, H. & Xiao, S. Frequency-tunable wide-angle polarization selection with a graphene-based anisotropic epsilon-near-zero metamaterial. *J. Opt.* **24**, 024004 (2022).
- Asgari, S. & Fabritius, T. Terahertz graphene-based multi-functional anisotropic metamaterial and its equivalent circuit model. *Sci. Rep.* **13**, 3433 (2023).
- Watts, C. M., Liu, X. & Padilla, W. J. Metamaterial electromagnetic wave absorbers. *Adv. Mater.* **24**, OP98–OP120 (2012).
- Xu, K.-D., Li, J., Zhang, A. & Chen, Q. Tunable multi-band terahertz absorber using a single-layer square graphene ring structure with T-shaped graphene strips. *Opt. Express* **28**, 11482–11492 (2020).
- Yi, Z. *et al.* Nanoribbon-ring cross perfect metamaterial graphene multi-band absorber in THz range and the sensing application. *Results Phys.* **14**, 102367 (2019).
- B.-Parizi, S. & Ebrahimi, A. Ultrathin, polarization-insensitive multi-band absorbers based on graphene metasurface with THz sensing application. *J. Opt. Soc. Am. B* **37**, 2372–2381 (2020).
- Zhou, Q., Liu, P., Bian, L. A., Cai, X. & Liu, H. Multi-band terahertz absorber exploiting graphene metamaterial. *Opt. Mat. Express* **8**, 2928–2940 (2018).
- Jain, P. *et al.* Graphene-based tunable multi-band metamaterial. *J. Mater. Sci. Mater. Electron.* **31**, 11878–11886 (2020).
- Wu, Z., Tian, J. & Yang, R. A graphene based dual-band metamaterial absorber for TE polarized THz wave. *Micro Nanostruct.* **168**, 207331 (2022).
- Aghaee, T. & Orouji, A. A. Reconfigurable multi-band, graphene-based THz absorber: Circuit model approach. *Results Phys.* **16**, 102855 (2020).
- Xiong, H., Ma, X., Liu, H., Xiao, D. & Zhang, H. Research on electromagnetic energy absorption and conversion device with four-ring multi-resistance structure. *Appl. Phys. Lett.* **123**, 153902 (2023).
- Deng, J.-H. *et al.* Metasurface-based microwave power detector for polarization angle detection. *IEEE Sens. J.* **23**, 22459–22465 (2023).
- Yang, Q. *et al.* Polarization-insensitive composite gradient-index metasurface array for microwave power reception. *Appl. Phys. Lett.* **122**, 253901 (2023).
- Singh, H. S. Super compact ultrathin quad-band with wide angle stability polarization independent metamaterial absorber. *Microw. Opt. Technol. Lett.* **62**, 718–725 (2019).
- Liu, Y. *et al.* Independently tunable multi-band and ultrawide-band absorbers based on multilayer metal-graphene metamaterials. *Opt. Express* **27**, 7393–7404 (2019).
- He, Y., Wu, Q. & Yan, S. Multi-band terahertz absorber at 0.1–1 THz frequency based on ultra-thin metamaterial. *Plasmonics* **14**, 1303–1310 (2019).
- Asgari, S. & Fabritius, T. Graphene-based multiband chiral metamaterial absorbers comprised of square split-ring resonator arrays with different numbers of gaps, and their equivalent circuit model. *IEEE Access* **10**, 63658–63671 (2022).
- Matthiakakis, N., Yan, X., Mizuta, H. & Charlton, M. D. B. Tuneable strong optical absorption in a graphene-insulator-metal hybrid plasmonic device. *Sci. Rep.* **7**, 7303 (2017).
- Zhou, Q. *et al.* Graphene based controllable broadband terahertz metamaterial absorber with transmission band. *Materials* **11**, 2409 (2018).
- Biabanifard, M., Asgari, S., Biabanifard, S. & Abrishamian, M. S. Analytical design of tunable multi-band terahertz absorber composed of graphene disks. *Optik* **182**, 433–442 (2019).
- Yao, G. *et al.* Dual-band tunable perfect metamaterial absorber in the THz range. *Opt. Express* **24**, 1518–1527 (2016).
- Kang, J., Shin, D., Bae, S. & Hong, B. H. Graphene transfer: key for applications. *Nanoscale* **4**, 5527–5537 (2012).
- Astorino, M. D. *et al.* Polarization-maintaining reflection-mode THz timelocal spectroscopy of a polyimide based ultra-thin narrow-band metamaterial absorber. *Sci. Rep.* **8**, 1985 (2018).
- Yi, Z. *et al.* Dual-band plasmonic perfect absorber based on graphene metamaterials for refractive index sensing application. *Micromachines* **10**, 443 (2019).
- Sarkar, R. *et al.* Independently tunable electromagnetically induced transparency effect and dispersion in a multi-band terahertz metamaterial. *Sci. Rep.* **9**, 18068 (2019).
- Cao, Y., Ruan, C., Chen, K. & Zhang, X. Research on a high-sensitivity asymmetric metamaterial structure and its application as microwave sensor. *Sci. Rep.* **12**, 1255 (2022).
- Asgari, S. & Fabritius, T. Multi-band terahertz metamaterial absorber composed of concentric square patch and ring resonator array. *Opt. Contin.* **3**, 148–163 (2024).
- McCall, J. Genetic algorithms for modelling and optimisation. *J. Comput. Appl. Maths.* **184**, 205–222 (2005).
- Liu, C. *et al.* Target driven design of electromagnetic metamaterial for dual-band Wi-Fi energy harvester. *Sens. Actuators A Phys.* **345**, 113815 (2022).
- Rahmanzadeh, M., Khavasi, A. & Rejaei, B. Analytical method for the diffraction of an electromagnetic wave by subwavelength graphene ribbons. *J. Opt. Soc. Am. B* **38**, 953–960 (2021).

34. Rahmanzadeh, M., Khavasi, A. & Rejaei, B. Analytical method for diffraction analysis and design of perfect-electric-conductor backed graphene ribbon metagratings. *Opt. Express* **29**, 28935–28952 (2021).
35. Rahmanzadeh, M., Rajabalipanah, H. & Abdolali, A. Multilayer graphene-based metasurfaces: Robust design method for extremely broadband, wide-angle, and polarization-insensitive terahertz absorbers. *Appl. Opt.* **57**, 959–968 (2018).
36. Cheng, D. K. *Field and Wave Electromagnetics*, Pearson Education (1989)
37. Andryieuski, A. & Lavrinenko, A. Graphene metamaterials based tunable terahertz absorber: Effective surface conductivity approach. *Opt. Express* **21**, 9144–9155 (2013).
38. Asgari, S. & Fabritius, T. Numerical simulation and equivalent circuit model of multi-band terahertz absorber composed of double-sided graphene comb resonator array. *IEEE Access* **11**, 36052–36063 (2023).
39. Xu, J. *et al.* Actively tunable linear and circular dichroic metamirrors based on single-layer graphene. *Opt. Express* **31**, 381–395 (2023).

Author contributions

S.A. has designed and developed the metamaterial under the supervision of T.F. S.A. has written the manuscript and T.F. has reviewed the manuscript.

Competing interests

The authors declare no competing interests.

Additional information

Correspondence and requests for materials should be addressed to S.A.

Reprints and permissions information is available at www.nature.com/reprints.

Publisher's note Springer Nature remains neutral with regard to jurisdictional claims in published maps and institutional affiliations.



Open Access This article is licensed under a Creative Commons Attribution 4.0 International

License, which permits use, sharing, adaptation, distribution and reproduction in any medium or format, as long as you give appropriate credit to the original author(s) and the source, provide a link to the Creative Commons licence, and indicate if changes were made. The images or other third party material in this article are included in the article's Creative Commons licence, unless indicated otherwise in a credit line to the material. If material is not included in the article's Creative Commons licence and your intended use is not permitted by statutory regulation or exceeds the permitted use, you will need to obtain permission directly from the copyright holder. To view a copy of this licence, visit <http://creativecommons.org/licenses/by/4.0/>.

© The Author(s) 2024